Conducting Polymetallorotaxanes: Metal Ion Mediated Enhancements in Conductivity and Charge Localization

S. Sherry Zhu[†,‡] and Timothy M. Swager*,[†]

Contribution from the Department of Chemistry, Massachusetts Institute of Technology, Cambridge, Massachusetts 02139, and Department of Chemistry, University of Pennsylvania, Philadelphia, Pennsylvania 19104

Abstract: In this paper we describe polymers of two metallorotaxane systems, Rot(**1**,M) and Rot(**2**,M) (M = Zn^{2+} or Cu^{1+}), which are formed by complexing a macrocyclic phenanthroline, a 5,5′-bis([2,2′-bithiophen]-5-yl)-2,2′-bipyridine (ligand **1**) or 5,5′-bis(3,4:3′,4′-bis(ethylenedioxy)[2,2′-bithiophen]-5-yl)-2,2′-bipyridine (ligand **2**), and Zn^{2+} or Cu^{1+} ions. The corresponding polymetallorotaxanes, PolyRot(**1**,M) and PolyRot(**2**,M), are produced by oxidative polymerization of Rot(**1**,M) and Rot(**2**,M). The investigations of the electrochemical, conducting, and optical properties of the metallorotaxanes and polymetallorotaxanes as well as related nonrotaxane polymers Poly(**1**) and Poly(**2**) are reported. The combined electrochemical and conductivity studies of PolyRot(**1**,M) and PolyRot(**2**,M) indicated that the polymetallorotaxane's redox and conducting properties were dramatically affected by the Lewis acidic and redox properties of the coordinated metal ions. The Lewis acidity produces charge localization and a redox conduction process in both polymetallorotaxane systems. The matching of the polymer and Cu$^{1+/2+}$ couple redox potentials in PolyRot(**2**,Cu) resulted in a Cu$^{1+/2+}$ contribution to conductivity. The metal-free PolyRot(**1**) and PolyRot(**2**) were produced by extracting the metal ions, and these polymers reversibly bound Zn^{2+} or Cu^{2+} ions in solution. The Cu^{2+} dopes the films of PolyRot(**2**) and Poly(**2**), which have lower oxidation potential than those of PolyRot(**1**), to produce 10^6−10^7-fold conductivity increases. In the case of PolyRot(**1**) and Poly(**1**), the rotaxane structure was demonstrated to be key for reversible complexation of metal ions.

Introduction

Conjugated polymer-based sensory schemes developed in our laboratory have made use of extended electronic communication between receptor sites to produce amplified responses for the detection of organic molecules and alkaline metal cations.[1−4] As part of our continued interest in the high sensitivity of a conjugated polymer's conductivity and/or fluorescence to analyte binding,[5,6] we are endeavoring to create highly conducting metallopolymers. Transition metals offer unique and desirable characteristics for the creation of sensory materials that are sensitive to anions as well as small molecules (CO, O$_2$, NO, etc.).[7,8] In spite of this and other potential applications, few studies have been directed at the development of transition metal/conducting polymer hybrid systems.[9−17] Additionally, in only a few of these cases was the metal directly interacting with the polymers.[9−15] Critical to their utility is the design of structures that enhance the electron transfer rate between metal centers relative to nonconjugated polymeric or molecular assemblies. The principles controlling electron transfer rates are largely unexplored, and there have been few studies that probe the ability of a conjugated polymer to mediate redox conductivity. Previous studies have investigated conducting polymers containing Ru(bpy)$_n$L$_{3−n}$,[14,15] ferrocene,[12] and transition metal ions.[16] In general, the results suggest that the redox conductivity is enhanced by a conjugated polymer. Systematic studies to optimize redox conductivity have only begun to appear.[15]

The creation of optimal conducting systems that actively utilize a transition metal's redox properties will most likely require extensive mixing of the metal-centered electronic states with those of the organic polymer. In our investigations we have targeted systems with well-defined structures that are capable of complexing both redox-active and redox-inactive metal ions. By making systematic comparisons between these materials, the relative contribution of the organic polymer and the metal-centered redox processes to the conductivity can be determined. To accomplish this, we have found the phenanthroline macrocycle developed by Sauvage and co-workers to be particularly useful for the formation of metallorotaxanes.[18]

[†] Massachusetts Institute of Technology.
[‡] University of Pennsylvania.
[⊗] Abstract published in *Advance ACS Abstracts,* December 1, 1997.
(1) Marsella, M. J.; Swager, T. M. *J. Am. Chem. Soc.* **1993**, *115*, 12214.
(2) Marsella, M. J.; Carroll, P. J.; Swager, T. M. *J. Am. Chem. Soc.* **1994**, *116*, 9347.
(3) Marsella, M. J.; Newland, R. J.; Carroll, P. J.; Swager, T. M. *J. Am. Chem. Soc.* **1995**, *117*, 9842.
(4) Marsella, M. J.; Carroll, P. J.; Swager, T. M. *J. Am. Chem. Soc.* **1995**, *117*, 9832.
(5) Zhou, Q.; Swager, T. M. *J. Am. Chem. Soc.* **1995**, *117*, 7017.
(6) Zhou, Q.; Swager, T. M. *J. Am. Chem. Soc.* **1995**, *117*, 12593.
(7) (a) Tovrog, B. S.; Drago, R. S. *J. Am. Chem. Soc.* **1974**, *96*, 6765. (b) Hoffman, B. M.; Szymanski, T.; Basolo, F. *J. Am. Chem. Soc.* **1975**, *97*, 637.
(8) (a) Cini, R.; Orioli, P. L. *J. Chem. Soc., Chem. Commun.* **1981**, 196. (b) Zanello, P.; Cini, R.; Cinquantini, A.; Orioli, P. L. *J. Chem. Soc., Dalton Trans.* **1983**, 2159.
(9) Zhu, S. S.; Carroll, P. J.; Swager, T. M. *J. Am. Chem. Soc.* **1997**, *118*, 8713.
(10) Zhu, S. S.; Swager, T. M. *Adv. Mater.* **1996**, *8*, 497.
(11) Wolf, M. O.; Wrighton, M. S. *Chem. Mater.* **1994**, *6*, 1526.
(12) Zotti, G.; Zecchin, S.; Schiavon, G.; Berlin, A.; Pagani, G.; Canavesi, A. *Chem. Mater.* **1995**, *7*, 2309.

(13) (a) Reddinger, J. L.; Reynolds, J. R. *Macromolecules* **1997**, *30*, 673. (b) Reddinger, J. L.; Reynolds, J. R. *Synth. Met.* **1997**, *84*, 225.
(14) (a) Peng, Z.; Yu, L. *J. Am. Chem. Soc.* **1996**, *118*, 3777. (b) Yamamoto, T.; Maruyama, T.; Zhou, Z.; Ito, T.; Fukuda, T.; Yoneda, Y.; Begum, F.; Ikeda, T.; Sasaki, S.; Takezoe, H.; Fukuda, A.; Kubota, K. *J. Am. Chem. Soc.* **1994**, *116*, 4832.
(15) Pickup, P. G.; Cameron, C. G. *Chem. Commun.* **1997**, 303.
(16) (a) Bidan, G.; Divisia-Blohorn, B.; Lapkowski, M.; Kern, J. M.; Sauvage, J. P. *J. Am. Chem. Soc.* **1992**, *114*, 5986. (b) Bidan, G.; Divisia-Blohorn, B.; Billon, M.; Kern, J. M.; Sauvage, J. P. *J. Electroanal. Chem.* **1993**, *360*, 189. (C) Kern, J. M.; Sauvage, J. P.; Bidan, G.; Billon, M.; Divisia-Blohorn, B. *Adv. Mater.* **1996**, *8*, 580.
(17) Deronzier, A.; Moutet, J. C. *Acc. Chem. Res.* **1989**, *22*, 249.

Scheme 1
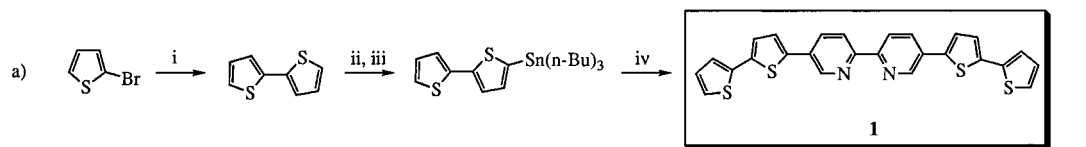
a) (i) Mg, ether, cat. Ni(dppp)Cl$_2$, Ar, 78%. (ii) n-BuLi, THF, -78 °C. (iii) (n-Bu)$_3$SnCl, THF, RT , 6h, Ar. (iv) 5,5'-dibromo-2,2'-bipyridine, cat. Pd(PPh$_4$)$_2$Cl$_2$, DMF, 80°-90°C, 10h, 60%.
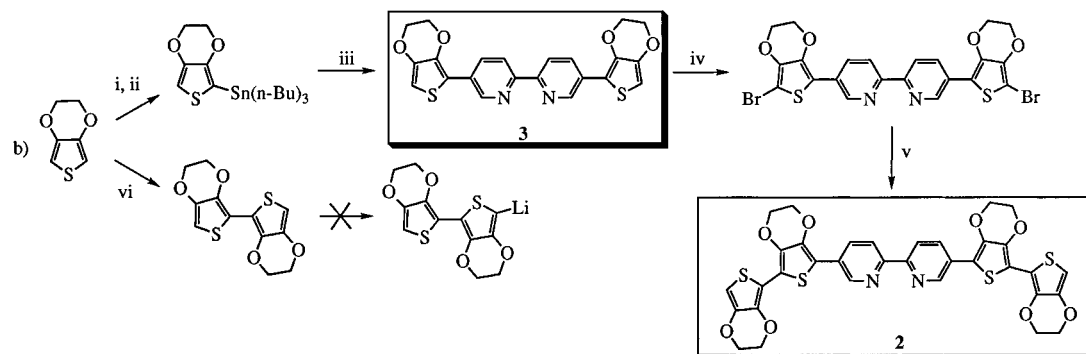

b) (i) and (ii) n-BuLi, THF, -78°C, 0.5 h. quenched with (n-Bu)$_3$SnCl, RT, 6 h, Ar. (iii) 5, 5'-dibromo-2, 2'-bipyridine, cat. Pd(PPh$_3$)$_2$Cl$_2$, DMF, 110°C, 12 h, Ar, 95%. (iv) NBS, DMF, RT, 12 h, Ar, (dark), 74%. (v) 2-(tributylstannyl)-3,4-ethylenedioxythiophene, cat. Pd(PPh$_3$)$_4$, DMF, Reflux, 6 h, Ar, (dark), 30-50%. (vi) TMEDA, n-BuLi, then Fe(acac)$_3$, THF, Reflux, 6 h, Ar, 97%.

In a previous communication,[9] we described two conducting polymetallorotaxanes, PolyRot(**1**,Zn) and PolyRot(**1**,Cu), which are formed from anodic polymerization of preassembled metallorotaxanes, Rot(**1**,Zn) and Rot(**1**,Cu). Once synthesized, the macrocycles are trapped on the polymer, presumably by physical or chemical cross-links, as they are retained after removal of the metal ion templates. This assembly of receptors allows for the investigation of polymers in complexed as well as metal-free states, and enables the determination of the contribution of metal ions to the electronic properties of the polymers. We found that both PolyRot(**1**,Cu) and PolyRot(**1**,Zn) displayed similar conducting properties which are attributed to the organic portion. Nevertheless, in the case of PolyRot(**1**,Cu), both metal- and polymer-based faradaic processes were observed. We further demonstrated that the structures may be reversibly converted between the metal-free PolyRot(**1**) and the PolyRot-(**1**,Zn) forms in CH$_3$CN solution.[9]

Reasoning that matching the polymer and copper-centered redox potentials would enhance the communication between these two elements, we have developed additional polymetal-lorotaxanes, PolyRot(**2**,Cu) and PolyRot(**2**,Zn), with 3,4-(ethylenedioxy)thiophene (EDOT) groups in place of thiophenes in the polymer backbone. The EDOT substitution makes the polymer much more electron-rich. Herein we report detailed synthetic, electrochemical, and optical studies of the polymetallorotaxanes, PolyRot(**1**,Cu), PolyRot(**1**,Zn), PolyRot(**2**,Cu), and PolyRot(**2**,Zn), and the corresponding metal-free polyrotaxanes, PolyRot(**1**) and PolyRot(**2**). We found that Zn^{2+} complexation induces charge localization and produces polymers with redox conductivity. The incorporation of EDOT units in PolyRot(**2**)-derived materials results in a matching of the Cu$^{1+/2+}$ redox couple with the potential at which the polymers are oxidized. This enables a 10^6-10^7 increase in conductivity by the complexation of Cu^{2+} ions. An additional outcome of this redox matching is that PolyRot(**2**,Cu) shows large Cu$^{1+/2+}$-

mediated conductivity whereas PolyRot(**1**,Cu) displayed no detectable conductivity which could be ascribed to the copper ions.

M = Zn^{2+}, PolyRot(**1**,Zn)
M = Cu^{1+}, PolyRot(**1**,Cu)

M = Zn^{2+}, PolyRot(**2**,Zn)
M = Cu^{1+}, PolyRot(**2**,Cu)
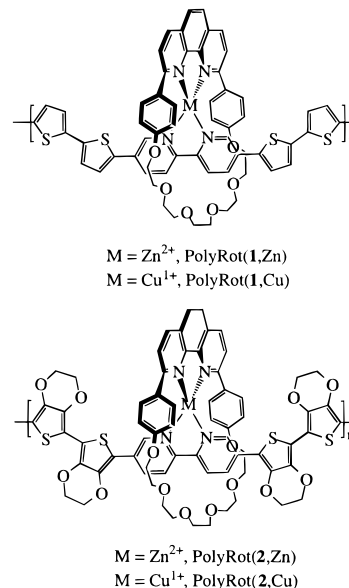
Results and Discussion

a. Syntheses and Characterization of Metallorotaxane Monomers. The bithienyl-substituted bipyridine **1** functions as a polymerizable monomer, a chelating component, and a threading element. We have previously demonstrated the utility of **1** in the formation of a conducting polymer, Poly(**1**), and related conducting polymer transition metal hybrid materials.[10] In our first attempt to produce a more electron-rich threading component, we synthesized 5,5′-bis(3,4-(ethylenedioxy)thien-2-yl)-2,2′-bipyridine (**3**) by a Stille coupling of 5,5′-dibromo-2,2′-bipyridine[19] with 2-(tributylstannyl)-3,4-(ethylenedioxy)-thiophene (Scheme 1). Although compound **3** can be oxidatively

(18) (a) Dietrich-Buchecker, C.; Sauvage, J. P. *Tetrahedron* **1990**, *46*, 503. (b) Sauvage, J. P. *Acc. Chem. Res.* **1990**, *23*, 321. (c) Armaroli, N.; Balzani, V.; Barigelletti, F.; Cola, L. D.; Flamigni, L.; Sauvage, J. P.; Hemmert, C. *J. Am. Chem. Soc.* **1994.** *116*, 5211.

(19) Whittle, C. P. *J. Heterocycl. Chem.* **1977**, *14*, 191.

Scheme 2
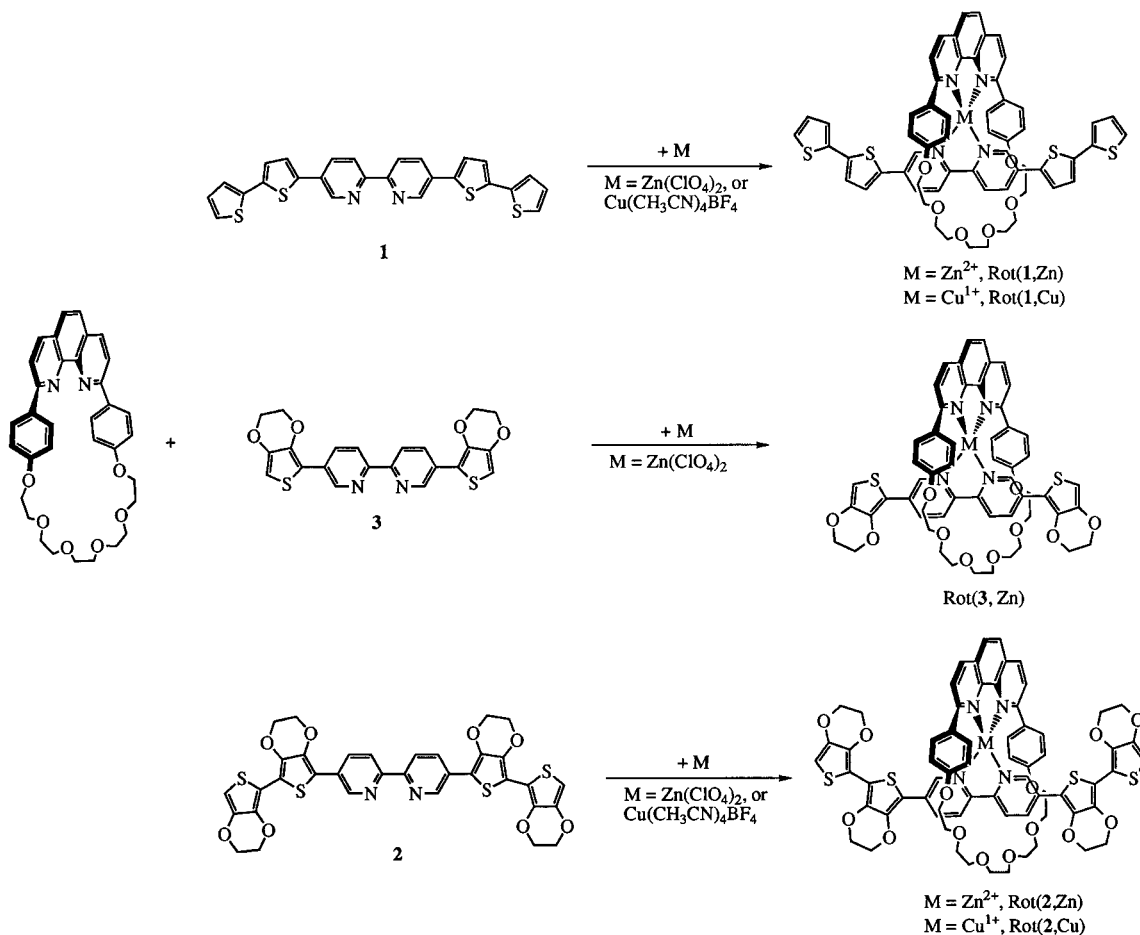
polymerized, we were unsuccessful at producing polymeric films from rotaxane complexes, Rot(**3**,Zn). We had experienced similar difficulties in other systems, which were eliminated by extending the thiophene segment.[10] Therefore, we synthesized an extended 3,4:3′,4′-bis(ethylenedioxy)[2,2′-bithiophen]-5-yl (BEDOT) substituted threading component, **2** (Scheme 1).


Poly(**1**)

Poly(**2**)
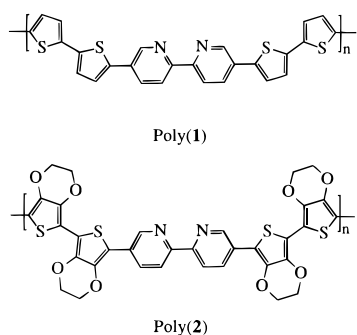
We initially attempted to synthesize compound **2** by a Stille coupling between 5,5′-dibromo-2,2′-bipyridine and 2-(tributylstannyl)-3,4:3,′4′-bis(ethylenedioxy)-5,5′-bithiophene. The highly electron-rich character of 3,4:3′,4′-bis(ethylenedioxy)-2,2′-bithiophene (BEDOT) apparently precludes an efficient preparation of 2-(tributylstannyl)-3,4:3′,4′-bis(ethylenedioxy)-5,5′-bithiophene by standard lithiation methods (Scheme 1). Thus, an alternative procedure was developed by brominating **3** with NBS. Stille coupling of 2-(tributylstannyl)-3,4-(ethylenedioxy)-thiophene with 5,5′-bis(5-bromo-3,4-(ethylenedioxy)thien-2-yl)-2,2′-bipyridine produced compound **2** in moderate yield (30−55%, depending on the scale). Compound **2** is an air- and light-

sensitive yellow-brown solid which rapidly decomposes on silica gel. Recrystallization from CH₂Cl₂/hexanes afforded pure compound **2** which was characterized by NMR and MS. Dilute CH₂Cl₂ solutions of **2** are bright yellow and display green emission.

We have previously described the syntheses and characterization of metallorotaxanes, Rot(**1**,Zn) and Rot(**1**,Cu) (Scheme 2).[9] A crystal structure determination of Rot(**1**,Zn) confirmed the formation of the metallorotaxane. UV−vis (Figure 1) and NMR are also diagnostic and indicate that Rot(**1**,Zn) and Rot(**1**,Cu) are fully associated in solution. Concurrent with the assembly of metallorotaxanes, the optical transitions of the threading component, **1** and **2**, display a pronounced red shift. Similar effects have been observed with protonation of other conducting polymers which have electron-poor pyridine groups alternating with more electron-rich moieties.[20b] The red shift suggests charge transfer character in the electronic transitions since protonation or metal coordination stabilizes negative charge transferred to the bipyridine residues in the excited state.[20] Also consistent with this description, the rotaxanes formed with more Lewis acidic Zn^{2+} display larger red shifts than those formed with Cu^{1+} (Figure 1). We also observed larger shifts in the rotaxanes assembled with **2** than those with **1**. Accordingly, the respective λ_{max} centered on the **1** and **2** moieties are red shifted by 60 and 80 nm in the Zn^{2+} rotaxanes and by 23 and 33 nm in the Cu^{1+} rotaxanes. ¹H and ¹³C NMR indicate complete formation of the rotaxanes in solution and the phenyl protons meta and ortho to the phenanthroline display respective

(20) (a) Fu, D.; Xu, B.; Swager, T. M. *Tetrahedron* **1997**, *53* (45), 15487. (b) Zhou, Z.; Maruyama, T.; Kanbara, T.; Ikeda, T.; Ichimura, K.; Yamamoto, T.; Kubota, K. *J. Chem. Soc., Chem. Commun.* **1991**, 1210.
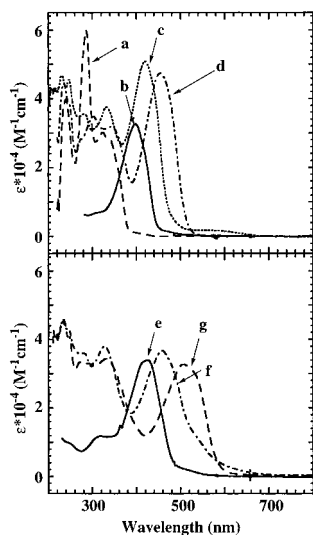
Figure 1. Top: UV−vis absorption of the phenanthroline macrocycle (dashed line, a), monomer **1** (solid line, b), Rot(**1**,Cu) (dotted line, c), and Rot(**1**,Zn) (dotted-dashed line, d) in CH$_2$Cl$_2$. Bottom: UV−vis absorption of monomer **2** (solid line, e), Rot(**2**,Cu) (dotted-dashed line, f), and Rot(**2**,Zn) (dashed line, g) in CH$_2$Cl$_2$.

upfield shifts from 7.16 and 8.40 ppm (CDCl$_3$) to 6.63 and 7.68 ppm (acetone-d_6) upon formation of Rot(**1**,Cu) and to 6.31 and 7.47 ppm on the formation of Rot(**2**,Cu). Numerous other Cu^{1+} complexation-induced shifts are observed in the other proton signals, and similar shifts are observed in the Zn^{2+} complexes.

b. Electrochemical Studies. All of the polymers investigated were synthesized by anodic electrochemical deposition. By this method, polymers can be deposited on microelectrode arrays for in situ cyclic voltammetry and relative conductivity measurements. Likewise deposition on an indium−tin−oxide (ITO) sheet enables UV−vis spectroelectrochemical measurements. Using techniques described elsewhere,[21] the conductivity is determined as a function of the applied electrochemical potential on the same functionalized electrodes that are used for cyclic voltammetry analysis. All electrochemical polymerization measurements were performed in 0.1 M (n-Bu)$_4$NPF$_6$/CH$_2$Cl$_2$ electrolyte solution in an air-free drybox under low-intensity lighting. A Ag wire was used as the quasi-reference electrode, and ferrocene ($E^{0\prime} = 0.40$ V) was used as a reference potential.

Typical thiophene-based conducting polymers exhibit cyclic voltammograms which are composed of broad unresolved waves indicating a high degree of delocalization.[22] Additionally, the conductivity profiles of thiophene-based conductors generally display a single window of conductivity for a given type of doping.[21] In polymers displaying redox-based conductivity, electrons hop between localized redox centers. For systems having equivalent structures and oxidation potentials, the rate of self-exchange (SE) electron transfer (ET) processes conforms to the simple equation $R_{SE} = k_{ET}[A][A^+]$, indicating a proportional relationship to the product of the concentrations of the reduced (A) and oxidized (A$^+$) species. This dictates that for a fixed amount of redox-active species ([A] + [A$^+$] = constant) the self-exchange rate between the oxidized and reduced states, and hence conductivity, will reach a maximum when the concentrations of the oxidized and reduced species are equal,

i.e., [A] = [A$^+$]. Thus, if a redox polymer's cyclic voltammogram exhibits multiple redox peaks, so too will the conductivity profile.[23]

The electrochemical and conducting properties of Poly(**1**) have been reported.[10] Poly(**1**) displays two unresolved oxidation peaks and resembles the behavior typical of polythiophene derivatives. Due to the electron-deficient character of its bipyridine moiety, Poly(**1**) is easier to reduce than polythiophene, and conductivity measurements indicate that Poly-(**1**) displays a stable conducting current in both p- and n-doping states.[10] As shown in Scheme 3, the corresponding metallorotaxane monomers, Rot(**1**,Zn) and Rot(**1**,Cu), are oxidatively polymerized to generate polymetallorotaxanes, PolyRot(**1**,Zn) and PolyRot(**1**,Cu).[9]

As expected, the oxidation potential required to polymerize **2** (polymerized by cycling the working electrode between −0.22 and +0.95 V) is lower than that required to polymerize **1** (cycling between −0.2 and +1.2 V). The resulting films of Poly(**2**) are dark purple in their reduced form. Electrochemical and conductivity measurements on films of Poly(**2**) using interdigitated microelectrodes show several interesting properties (Figure 2a). The cyclic voltammogram of Poly(**2**) displays two oxidation waves (Table 1 and Figure 2a) with almost equal peak currents. A linear relationship between the peak currents and scan rate confirms that the electroactive species are surface confined. The conductivity profile shows the first maximum to be at the same potential as the first oxidation wave. After passing through the first wave, a slight drop in the conductivity is observed before reaching a second maximum ($\sigma = 3.5 \times 10^{-2}$ S/cm) at the half-wave potential of the second oxidation wave. In other words, the conductivity of Poly(**2**) results from two discrete redox waves which produce two windows of peak conductivity. This correspondence between redox processes and the conductivity suggests that Poly(**2**) behaves as a charge-localized redox conductor.
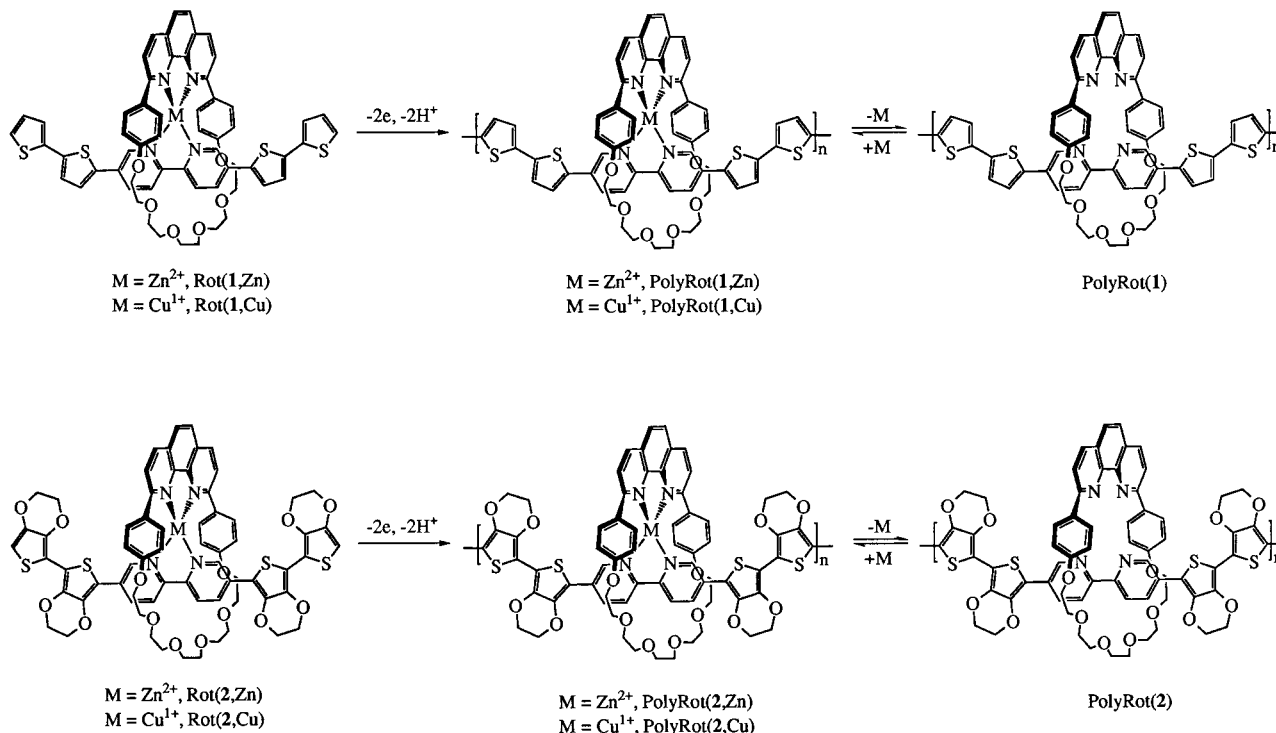
Considering that the electrochemical polymerization process produces protons, we suspected that the as-synthesized film of Poly(**2**) may be protonated. Indeed, rinsing films of Poly(**2**) with base (ethylenediamine) immediately transformed the films to a red color and also produced a broader and less defined cyclic voltammogram. As shown in Figure 2b, the cyclic voltammogram still displays the two oxidation waves and two conductivity maxima after ethylenediamine treatment. However, deprotonation results in a negative shift of the oxidation potentials (Table 1), indicating that the neutralized polymer is easier to oxidize. Base treatment also changes the shape of the conductivity profile, and we observed a decrease in the first conductivity wave and a slight conductivity increase commensurate with the second oxidation wave.

As we have reported previously,[9] PolyRot(**1**,Zn) displays a cyclic votammogram with two partially resolved one-electron waves. Additionally, the conductivity exhibits the characteristics of a localized redox system with conductivity peaks ($\sigma_{max} = 3.7 \times 10^{-4}$ S/cm) corresponding directly with the half-wave potentials. PolyRot(**1**,Cu) displays two less resolved waves similar to those of PolyRot(**1**,Zn) and an additional Cu$^{1+/2+}$ wave at a less positive potential. The Cu$^{1+/2+}$ wave displays a large hysteresis ($\Delta E_p = E_{pc} - E_{pa} = 118$ mV at 50 mV/s), and due to this kinetic sluggishness, no measurable redox conductivity was associated with the Cu$^{1+/2+}$ wave.

The polymetallorotaxanes formed with **2** display interesting electrochemical behaviors which are dramatically influenced by metal ion complexation. Electrolyte solutions of either Rot-

(21) (a) Kittlesen, G. P.; White, H. S.; Wrighton, M. S. *J. Am. Chem. Soc.* **1984**, *106*, 7389. (b) Ofer, D.; Crooks, R. M.; Wrighton, M. S. *J. Am. Chem. Soc.*. **1990**, *112*, 7869. (c) Paul, E. W.; Ricco, A. J.; Wrighton, M. S. *J. Phys. Chem.* **1985**, *89*, 1441. (d) Thackeray, J. W.; White, H. S.; Wrighton, M. S. *J. Phys. Chem.* **1985**, *89*, 5133.
(22) *Handbook of Conducting Polymers*; Skotheim, T. J., Ed.; Dekker: New York, 1986.

(23) *Electroactive Polymer Electrochemistry*; Lyons, M. E. G., Ed.; Plenum Press: New York, 1994; see also references therein.

Scheme 3

M = Zn^{2+}, Rot(**1**,Zn)
M = Cu^{1+}, Rot(**1**,Cu)

M = Zn^{2+}, PolyRot(**1**,Zn)
M = Cu^{1+}, PolyRot(**1**,Cu)

PolyRot(**1**)

M = Zn^{2+}, Rot(**2**,Zn)
M = Cu^{1+}, Rot(**2**,Cu)

M = Zn^{2+}, PolyRot(**2**,Zn)
M = Cu^{1+}, PolyRot(**2**,Cu)

PolyRot(**2**)

Table 1. Apparent Formal Reduction Potential $E^{0\prime}$ (V vs Ag Wire)^a of the Two Redox Processes of Each Polymer

	$E^{0\prime}$ (V) (polymers)		$E^{0\prime}$ (V) (metal-free polyrotaxanes)	
Poly(**1**)	1.12	1.29		
Poly(**2**)	0.43 (0.34)^b	0.79 (0.74)^b		
PolyRot(**1**,Zn)	0.96	1.24	0.96−1.24^c	
PolyRot(**1**,Cu)	0.98	1.26	0.98−1.26^c	
PolyRot(**2**,Zn)	0.41	0.74	0.36	0.64
PolyRot(**2**,Cu)	0.49^c	0.79	0.41	0.71

^{a} $E^{0\prime} = (E_{pa} + E_{pc})/2$. ^{b} Values in parentheses are for the material after treatment with ethylenediamine. ^{c} After base treatment, the two polymer-based redox peaks lose their definition and give a broad redox wave over the indicated potential region.
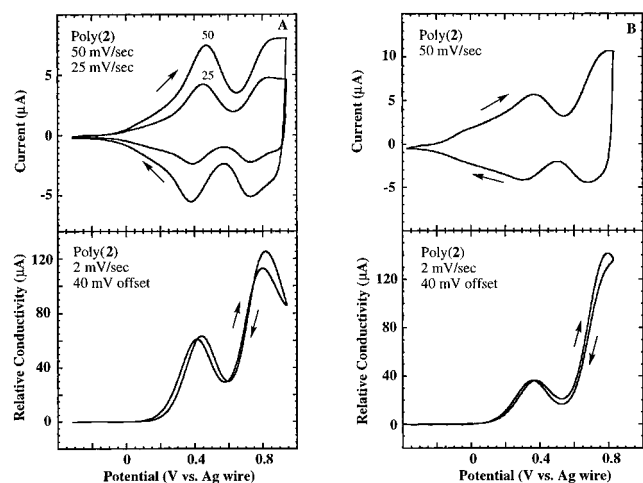
Figure 2. Columns A and B show the cyclic voltammograms (top) and relative conductivity profiles (bottom) of Poly(**2**) on interdigitated electrodes. (a) Poly(**2**) film as synthesized. (b) Poly(**2**) after treatment with base (ethylenediamine).

(**2**,Zn) (0.77 mM) or Rot(**2**,Cu) (0.46 mM) were electrochemically polymerized by cycling between −0.4 and +1.15 V to generate green-blue films. As shown in Figure 3, a striking
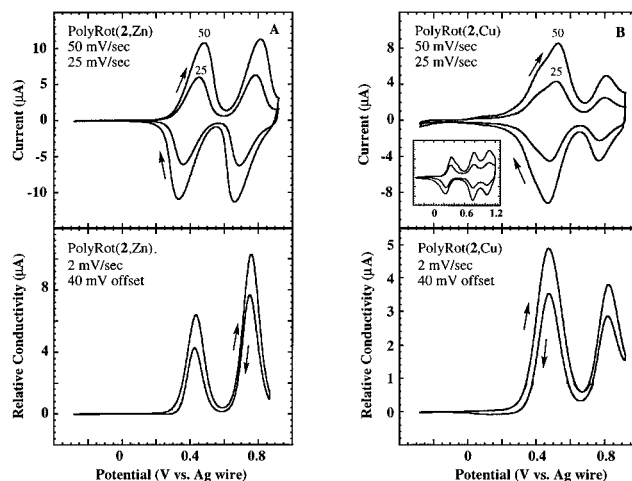
Figure 3. Column A: cyclic voltammograms (top) and conductivity profile (bottom) of PolyRot(**2**,Zn) on interdigitated electrodes. Column B: cyclic voltammograms (top) and conductivity profile (bottom) of PolyRot(**2**,Cu) on interdigitated electrodes. Cyclic voltammograms of PolyRot(**1**,Cu) at 25 and 50 mV/s scan rates are shown as an inset in (B, top) for comparison.

feature of the cyclic voltammogram is the well-resolved localized nature of the redox waves. Both PolyRot(**2**,Zn) and PolyRot(**2**,Cu) display behavior typical of reversible surface-confined localized redox sites with small ΔE_p and a linear relationship between the scan rate and peak currents. PolyRot-(**2**,Zn) displays two polymer-based redox peaks with equal peak currents (Figure 3a). The relative conductivity (current) of PolyRot(**2**,Zn) correlates with this electroactivity and reaches a local maximum at the half-wave potential of the first oxidation peak. The conductivity then drops nearly to a baseline level before rising to its highest level ($\sigma = 6.8 \times 10^{-4}$ S/cm) at a potential which is coincident with the second redox wave. From these cyclic voltammogram and conductivity investigations we conclude that PolyRot(**2**,Zn) behaves as a redox conductor with rapid electron transfer between localized redox states in the polymer backbone. The localized redox conductor character-
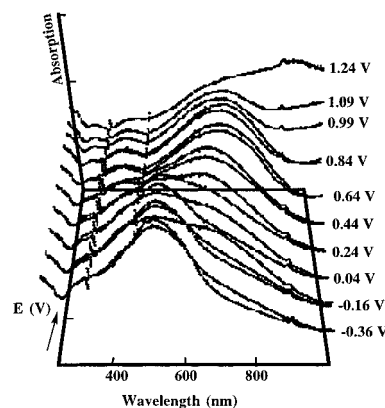
istics are more pronounced in PolyRot(**2**,Zn) than in Poly(**2**), which indicates that the complexation of Zn^{2+} ions results in enhanced charge localization in the polymer backbone. We also note that PolyRot(**2**,Zn)'s behavior is consistent with the behavior of Poly(**2**) which displays more localized behavior in its protonated form.

PolyRot(**2**,Cu) displays two oxidation waves in its cyclic votammogram (Figure 3). A comparison with the electrochemical behavior of PolyRot(**1**,Cu), shown as an inset in Figure 3, top, illustrates how the electron-rich character of the Poly(**2**) backbone produces a negative shift of the two polymer-centered oxidation peaks to a region which overlaps with the $Cu^{1+/2+}$ wave. This results in a 0.49 V wave that is approximately twice as large as the wave at higher potential. Close inspection indicates that the former contains two unresolved waves. The conductivity profile of PolyRot(**2**,Cu) shown in Figure 3 is also indicative of redox behavior. However, this behavior is different from that of PolyRot(**2**,Zn) in that the first conducting peak ($\sigma = 1.3 \times 10^{-3}$ S/cm) for PolyRot(**2**,Cu) is now considerably larger than the second peak. This last feature is significant since our investigations of PolyRot(**1**,Zn), PolyRot(**1**,Cu), PolyRot-(**2**,Zn), Poly(**1**), and Poly(**2**) consistently show a smaller relative conductivity associated with the wave at lower potential and maximum at higher potential. The $Cu^{1+/2+}$ waves in both PolyRot(**1**,Cu) and PolyRot(**2**,Cu) also provide an internal Coulometric reference, which indicates that the threading polymers (i.e., Poly(**1**) and Poly(**2**)) of the polyrotaxanes exhibit two sequential one-electron oxidation processes for each repeating unit.

c. Optical Studies. Given the interesting redox and conduction behaviors of these materials, we have performed in situ UV−vis spectroscopy as a function of applied electrochemical potential. Spectroelectrochemical measurements were carried out in a home-built sealed cell using indium−tin−oxide (ITO) as a working electrode. The UV−vis absorption spectra were measured at electrochemical potentials chosen to interrogate the nature of the polymer. To confirm that the polymer had come to an equilibrium at each potential, we performed measurements in both the oxidative cycle and the subsequent reductive cycle. The spectra at each potential were nearly the same for both cycles, confirming that the films were in equilibrium with the electrodes.

It has been reported by others that polythiophene and poly-(EDOT) show strong interband absorptions with λ_{max} at 480 and 511 nm, respectively.[24] Upon doping, the intensity of this interband transition was found to decrease, and two new absorption peaks appear at lower energies.[24] With increasing doping levels, the interband absorption peaks disappear and the two low-energy absorption peaks gain intensity and eventually merge. In the heavily doped state, the spectra show increasing intensity at long wavelengths that extend into the near-IR. This latter feature is generally considered to be characteristic of free carriers in the metallic state and is referred to as a free carrier tail.[24]

The UV−vis spectra of Poly(**2**) are very different from those of simple polythiophene derivatives. As shown in Figure 4, the as-synthesized dark purple films of Poly(**2**) exhibit a broad absorption with two unresolved intensity maxima at 540 and 680 nm. After treatment with base (ethylenediamine), the film appears red and displays a well-defined absorption peak centered at 540 nm. This optical change further confirms our earlier assertion that the Poly(**2**) is protonated during oxidative polymerization. A similar change in the UV−vis spectra of Poly-

(24) (a) Patil, A. O.; Heeger, A. J.; Wudl, F. *Chem. Rev.* **1988**, *88*, 183. (b) Chen X.; Inganäs, O. *J. Phys. Chem.* **1996**, *100*, 15202.

Figure 4. UV−vis absorption of Poly(**2**) on ITO glass as a function of the applied electrochemical potential.

(**2**) is also achieved by holding the potential of the dark purple films at −0.36 V for 20 min, indicating that reducing potentials can also affect deprotonation. Presumably, in this case the supporting electrode surface or other generated species remove the protons. Due to an erosion of the electrochemical behavior of Poly(**2**) on ITO after ethylenediamine treatment, we have used this reductive method to deprotonate the polymer. The neutral form of Poly(**2**) displays an interband transition at 540 nm, which is to the red of both polythiophene and poly(EDOT). This bathochromic shift is due to the alternating donor−acceptor structure ((EDOT)$_4$ = donor, bipyridine = acceptor) of Poly-(**2**) which creates a lower energy charge transfer absorption. With initial oxidation, a single lower energy absorption appears at 670 nm. This new band grows at the expense of the 540 nm peak, and at an applied potential of 0.64 V (a state between the first and the second oxidation waves), the interband absorption is absent and the dominant feature is a broad absorption at 706 nm. Increasing the applied oxidation potential to 0.84 V, which corresponds to the center of the second oxidation wave and the point of the highest conductivity, gives a spectrum with the 706 nm absorption displaying the same intensity and a new absorption tail from approximately 880 into the near-IR. At a potential of 1.24 V, where the conductivity is low, a feature is observed that resembles a typical free carrier tail extending into the near-IR. This result is in stark contrast to those of polythiophene derivatives and other conducting polymers which display this spectroscopic feature in their highly conducting states. Thus, it is surprising that the free-carrier tail is largest in the low conductivity state. On the return (reductive) scan from +1.24 to −0.36 V, the absorption shows some hysteresis (Figure 4). This effect appears to be the result of a small amount of protonation of Poly(**2**) with oxidation, which results from a reversal of the initial reductive treatment. The spectrum of neutral Poly(**2**) is again recovered after reducing Poly(**2**) at −0.36 V for 20 min.

The interaction of the Poly(**2**) backbone with Zn^{2+} and Cu^{1+} in the polymetallorotaxane systems produces effects similar to those reported for the monomers in Figure 1. In their undoped form, PolyRot(**2**,Zn) and PolyRot(**2**,Cu) display absorption maxima at 630 and 618 nm, respectively (Figure 5), which are considerably red shifted from the 540 nm maximum of Poly-(**2**). The bipyridine moiety is a stronger acceptor when complexed with Zn^{2+} ions as compared to Cu^{1+} ions, and consistently the PolyRot(**2**,Zn) shows a larger red shift. The UV−vis spectral changes observed as a function of applied electrochemical potential for PolyRot(**2**,Cu) and PolyRot(**2**,Zn) are similar. As shown in Figure 5, these materials differ from Poly(**2**) in that the peaks which correspond to the initial absorption maxima remain throughout the entire cycle. Similar
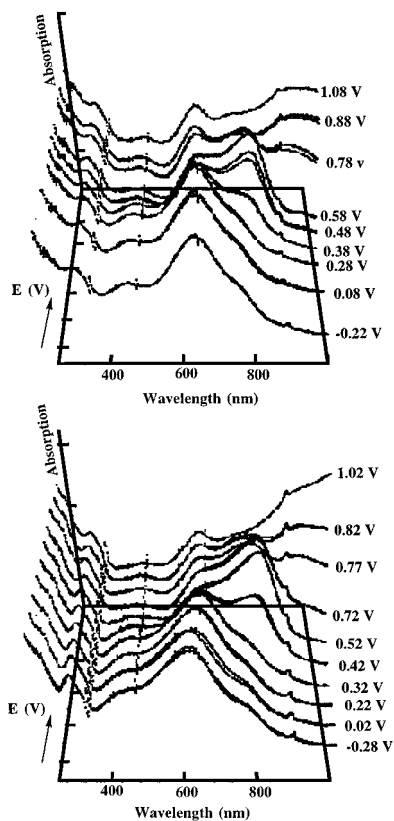
Figure 5. UV−vis absorption as a function of applied electrochemical potentials. Top: PolyRot(**2**,Zn). Bottom: PolyRot(**2**,Cu). Note the nearly identical spectra obtained in both oxidation and reduction cycles.

Figure 6. Top: cyclic voltammograms of PolyRot(**1**,Zn) (solid line); after treatment with base to form polyRot(**1**) (dotted-dashed line), and then immersed in Zn(ClO$_4$)$_2$/CH$_3$CN (dotted line). Bottom: metal-free PolyRot(**1**) after treatment with a CuBF$_4$(CH$_3$CN)$_4$/CH$_3$CN solution.

to Poly(**2**), at intermediate and high oxidation levels a new peak appears at lower energy and a feature resembling a free carrier tail absorption dominates the spectra at the highest oxidation potentials. Also consistent with the behavior of Poly(**2**), both PolyRot(**2**,Cu) and PolyRot(**2**,Zn) are in their lower conducting states when the new absorption tails which extended into the near-IR are at their highest intensity.

d. Reversible Complexation of Metal Ions. Polyrotaxanes with preorganized binding sites are potential sensory materials for transition metal ions. Critical to the sensory properties of conducting polyrotaxanes is the reversibility of metal ion binding. We have demonstrated the reversible binding of Zn^{2+} to metal-free PolyRot(**1**) through optical absorption changes.[9] Noting that the UV−vis spectrum only reflects the changes in local electronic structure,[25] we have further investigated the effects of interaction between polyrotaxane and the metal ions on the conductivity, which is a collective property. As shown in Figure 6, the cyclic voltammogram of PolyRot(**1**,Zn) films displays two well-defined oxidation waves. Upon extraction of the Zn^{2+} with base (ethylenediamine) treatment, the two oxidation waves lose definition and form a broad oxidation wave. Meanwhile, the UV−vis spectrum displays a blue shift of the interband absorption, indicating generation of metal-free PolyRot(**1**). Immersion of PolyRot(**1**) in a saturated MeCN of Zn^{2+} solution again produces PolyRot(**1**,Zn) with two unresolved oxidation waves and a red shift of the polymer-based UV−vis absorption (Figure 6). The partial recovery of the oxidation peaks suggests that the PolyRot(**1**) is only partially complexed with Zn^{2+} ions. The weak binding effect probably results from the flexibility of the macrocycles to rotate or slide along the threading polymers after removal of the metal ions. Immersion of PolyRot(**1**) into saturated Cu^{1+} or Cu^{2+} solutions
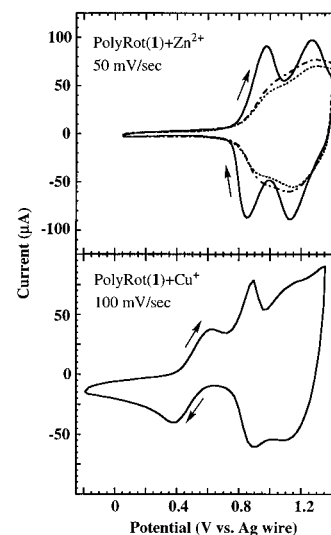
produces a similar red shift in the UV−vis absorption. The cyclic voltammogram of PolyRot(**1**) after treatment with Cu^{2+} only exhibits a very small peak at 0.49 V corresponding to the Cu^{1+}/Cu^{2+} redox couple. The Cu^{1+}-treated PolyRot(**1**), however, produces a relatively large redox wave at 0.49 V associated with an electrochemically irreversible peak (Figure 6). It is apparent that PolyRot(**1**) has a higher affinity for Cu^{1+} with respect to Cu^{2+}, which is to be expected for the polyrotaxane structure with preassembled tetrahedral binding sites. Dipping the macrocycle-free Poly(**1**) in Cu^{2+} solutions broadens the absorption spectrum, but no visible Cu$^{1+/2+}$ wave appears in the cyclic voltammogram. The interaction of Poly(**1**) with Cu^{1+} solutions produces neither an absorption change nor a Cu$^{1+/2+}$ redox wave in the cyclic voltammogram. Thus, the rotaxane structure is key to metal binding, and Poly(**1**) shows no evidence of Zn^{2+} binding under the same conditions.[9]

In the case of the PolyRot(**2**) system, the contribution of the copper ion to the conductivity of PolyRot(**2**,Cu) makes this a particularly interesting system to study the reversible binding of Cu^{1+} and Cu^{2+}. Our investigations of Cu^{1+} and Cu^{2+} complexation by PolyRot(**2**) have focused on electrochemical and conductivity studies.

Metal-free PolyRot(**2**) is produced by ethylenediamine extraction of the metal ion from PolyRot(**2**,Cu) or PolyRot(**2**,Zn). The green-blue films of PolyRot(**2**,Cu) and PolyRot(**2**,Zn) turn red after ethylenediamine treatment, and electrochemistry displays features similar to those of Poly(**2**) (Figures 7a and 8a), suggesting the formation of metal-free PolyRot(**2**). The relative conductivity of PolyRot(**2**) is higher than those of PolyRot(**2**,-Zn) and PolyRot(**2**,Cu), indicating that the increased flexibility in the metal-free structure allows for greater interchain interactions. UV−vis spectroscopy of PolyRot(**2**) shows absorptions from the macrocycle phenanthroline between 250 and 400 nm after removal of the metal ions, thereby confirming that the rotaxane structures persist. The green-blue color is restored after dipping the metal-free PolyRot(**2**) into a saturated Cu(BF$_4$)$_2$/CH$_3$CN solution. As shown in Figures 7b and 8b, cyclic voltammograms of the reconstituted PolyRot(**2**,Cu) are the same as those for PolyRot(**2**,Cu) obtained from the polymerization of Rot(**2**,Cu). Also apparent from Figures 7 and 8 is the fact that the same material is formed regardless of which polyrotaxane is the starting material, PolyRot(**2**,Zn) or PolyRot(**2**,-Cu). The conductivity profiles shown in Figure 7 indicate some

(25) Thienpont, H.; Rikken, G. L. J. A.; Meijer, E. W.; Tenhoeve, W.; Wynberg, H. *Phys. Rev. Lett.* **1990**, *65*, 2141.
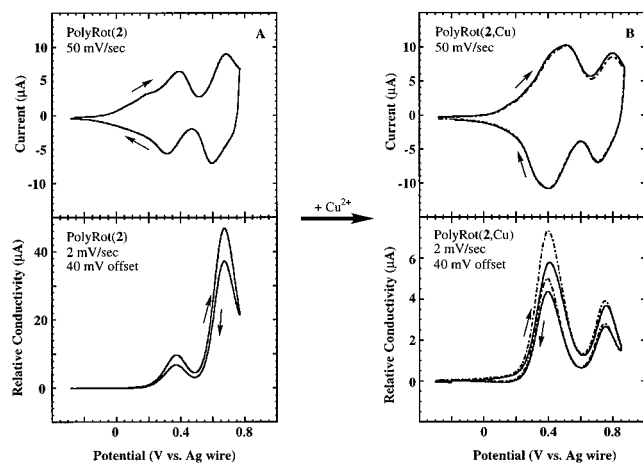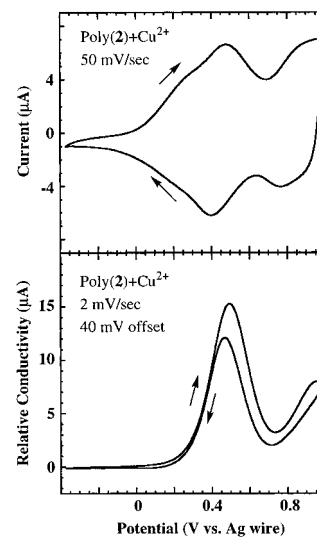
Figure 7. Column A: cyclic voltammogram (top) and relative conductivity profile (bottom) of PolyRot(**2**) formed by treatment of PolyRot(**2**,Zn) with ethylenediamine. Column B: cyclic voltammograms (top) and relative conductivity profiles (bottom) of PolyRot(**2**) after dipping in Cu(BF$_4$)$_2$/CH$_3$CN solution to generate PolyRot(**2**,Cu): the first scan (solid line); the third scan (dotted-dashed line).
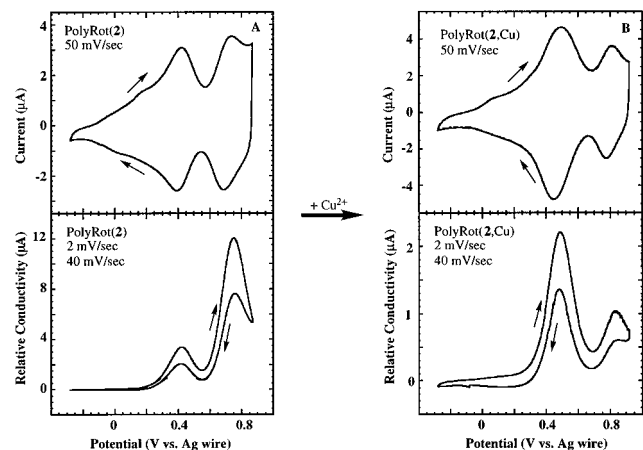
Figure 8. Column A: cyclic voltammogram (top) and relative conductivity profile (bottom) of PolyRot(**2**,Cu) after treatment with ethylenediamine to form PolyRot(**2**). Column B: cyclic voltammogram (top) and relative conductivity profile (bottom) of PolyRot(**2**) after dipping in Cu(BF$_4$)$_2$/CH$_3$CN solution to generate PolyRot(**2**,Cu).

structural evolution since the conductivity of the third scan is larger than that of the first scan. However, cyclic voltammetry displays identical behavior over several cycles. This last point speaks to the high sensitivity of conductivity to minor differences in a material. Both the electronic and structural properties of PolyRot(**2**) contribute to its strong affinity for Cu^{2+} ions. Recall that PolyRot(**1**) does not display a high affinity for Cu^{2+}. The electron-rich and bulky EDOT moiety enhances the chelating ability of PolyRot(**2**) by increasing the basicity of the bipyridine and by biasing the macrocycle to prefer bipyridyl sites along the threading polymer. Thus, the EDOT-based polyrotaxane likely maintains rigid preorganized coordination sites and displays a qualitatively higher binding constant than PolyRot(**1**). We also investigated the interaction of PolyRot-(**2**) in a saturated Zn^{2+}/MeCN solution. As expected, treating the PolyRot(**2**) with Zn^{2+} ions shifts the cyclic voltammogram such that it coincides with that of as-synthesized PolyRot(**2**,-Zn), which indicates the reconstruction of PolyRot(**2**,Zn). This result is consistent with PolyRot(**1**), which reversibly binds Zn^{2+} ions in MeCN solution.

For comparison, we conducted the same Cu^{2+} and Zn^{2+} treatment with neutral Poly(**2**), which has no macrocyclic component. In contrast to what we observed for Poly(**1**), the

Figure 9. Cyclic voltammogram (top) and relative conductivity profile (bottom) of Poly(**2**) on an interdigitated microelectrode after treatment with base (ethylenediamine) and followed by complexation with Cu^{2+} ions on interdigitated microelectrodes.

films of Poly(**2**) turned blue after dipping into Cu^{2+} solution. Although the cyclic voltammogram and conductivity profiles are similar to those of PolyRot(**2**,Cu) (Figure 9), close inspection reveals that the second oxidation wave is 120 mV more positive than that of PolyRot(**2**,Cu). Treating Poly(**2**) with Zn^{2+} ions revealed that neutral Poly(**2**) also binds Zn^{2+} to produce a positive shift of the cyclic voltammograms to the potentials near which the protonated Poly(**2**) was oxidized. These results imply that **2** is a stronger chelating ligand than **1**. However, the difference between the electrochemistry of Cu^{2+}-treated Poly-(**2**) and PolyRot(**2**,Cu) indicates that the binding mode is different in Poly(**2**,Cu). Considering that nitrogen, sulfur, and oxygen are all good donors, a variety of binding modes can exist. One possibility is interchain coordination of Cu^{2+}; however, it will be difficult to elucidate the binding modes.

As mentioned in the Introduction, the close match of the oxidation potentials of the Cu$^{1+/2+}$ couple and Poly(**2**) or PolyRot(**2**) enables the polyrotaxanes to be oxidatively doped with Cu^{2+} binding. Since complexation and oxidation of the polyrotaxanes by Cu^{2+} will transform the insulated polyrotaxanes to conducting polymetallorotaxanes, the polymer's resistance should dramatically change. To detect these changes in resistance, we used an electrometer to measure the resistance of the undoped PolyRot(**2**,Zn) deposited on the interdigitated electrodes. We also measured the resistance changes after removal of Zn^{2+} ions to form PolyRot(**2**) and in doped PolyRot-(**2**,Cu) formed by treatment with Cu^{2+} ions. The polymer films were taken out of the electrolyte solutions and dried under vacuum for 10 min before resistance measurements were performed.

The blank interdigitated microelectrodes exhibited 1×10^{12} Ω resistance, and when the electrodes were coated with undoped PolyRot(**2**,Zn) films, the resistance dropped to 7.0×10^9 Ω. Removal of the Zn^{2+} ions to give PolyRot(**2**) increased the resistance slightly to 4.0×10^{10} Ω. More significantly, however, the resistance dropped dramatically to 3.2×10^4 Ω after treating PolyRot(**2**) with Cu^{2+} solution. Cyclic voltammetry and conductivity measurements confirm the formation of PolyRot(**2**,Cu). Thus, Cu^{2+} complexation to PolyRot(**2**) produces a $>10^6$-fold increase in conductivity. This result suggests that the PolyRot(**2**) backbone is oxidized by Cu^{2+} ions to generate PolyRot(**2**,Cu) with charge carriers in the polymer backbone. In a control experiment, we have shown PolyRot-

(**2**) shows less than a 10-fold change in resistance after treatment with Cu^{1+} or Zn^{2+} ions. In a similar resistance experiment, PolyRot(**1**), which has higher oxidation potential than PolyRot-(**2**), only produces a 10^2-fold resistance decrease when interacting with Cu^{2+}.

Similar resistance measurements were carried out on macrocycle-free Poly(**2**) and Poly(**1**). The same electrode coated with a protonated film of Poly(**2**) displayed a resistance of 2.3 $\times 10^6$ Ω. Removal of the protons increased the resistance to 2.6×10^{10} Ω. Treatment with Cu^{2+} results in a resistance as small as 1.0×10^3 Ω (a drop of $>10^7$), which again suggests that Cu^{2+} is not only functioning as a Lewis acid but also doping Poly(**2**). However, Poly(**1**) only generates a 10^2-fold decrease in resistance when interacting with Cu^{2+} ions. This further demonstrates that the doping of the polymer by Cu^{2+} is the major contribution to the conductivity increase in Poly(**2**).

Conclusions

We have described the syntheses, UV−vis spectroscopy, electrochemistry, and conducting properties of conducting polymetallorotaxanes containing Zn^{2+} and Cu^{1+} and their corresponding metal-free polyrotaxanes. In all the polymetallorotaxanes, we observe two discrete redox processes which are associated with two conductivity maxima. For PolyRot(**1**,Cu), the $Cu^{1+/2+}$ redox couple produces no measurable conductivity. However, in the redox matched PolyRot(**2**,Cu), the $Cu^{1+/2+}$ redox couple gives greatly enhanced conductivity. The Cu^{2+} treatment of metal-free PolyRot(**2**) readily regenerates PolyRot-(**2**,Cu), which also exhibits a $Cu^{1+/2+}$-mediated conductivity enhancement.

The spectroelectrochemistry displays trends which are different from those of typical conducting polymers. An important deviation from other systems is that the polymers investigated show a low conductivity in their highest oxidation level but at the same time display absorption features which resemble free-carrier states.

By measuring the resistance changes of the metal-free PolyRot(**2**) and Poly(**2**) before and after Cu^{2+} treatment, we demonstrated that Cu^{2+} binds and dopes these polymers to produce a 10^6- to 10^7-fold increase in the polymer's conductivity. The observation of such large metal-mediated conductivity enhancements suggests a new approach to sensory schemes for the detection of a variety of transition metal ions.

Experimental Section

General Procedures. Air- and moisture-sensitive reactions were carried out in oven-dried glassware using standard Schlenk techniques under an inert atmosphere of dry argon. Dry DMF was used from Aldrich Kilo-lab metal cylinders or sure-seal bottles. Anhydrous CH_2Cl_2 and CH_3CN used for electrochemistry studies were obtained from Aldrich as sure-seal bottles. 3,4-(Ethylenedioxy)thiophene (EDOT) was obtained from Bayer, and other reagents were used as received from Aldrich unless otherwise noted. NMR spectra were recorded with a Bruker AC-250 (^{1}H) or Varian 500 MHz (^{1}H and ^{13}C) spectrometer. UV−vis absorption spectroscopy was performed on a Hewlett-Packard 8453 diode array spectrophotometer. Resistances of dried films were measured on an interdigitated electrode using a Keithley Instruments solid state electrometer, model 610CR. Electrochemical measurements were performed in an air-free drybox under reduced lab lighting using a computer-controlled Autolab Model PGSTAT 20 potentiostat from Eco Chemie. All electrochemical measurements shown were performed on interdigitated array microelectrodes purchased from AAI-ABTECH and having an interelectrode spacing of 5 μm. The electrolyte solutions used for all electrochemistry and conductivity measurements were 0.1 M (n-Bu)$_4$NPF$_6$ in CH_2Cl_2, and all electrochemical potentials are reported relative to an isolated silver wire quasi-reference electrode. Because of the instability of the Ag wire quasi-reference electrode in

the CH_2Cl_2 electrolyte solution, the potentials of all cyclic voltammograms obtained were checked for accuracy by adding ferrocene as the reference compound in the same electrolyte medium used for the electrochemical studies. The electrochemical potentials were corrected such that the $E^{0\prime}$ of ferrocene is 0.40 V in 0.1 M (n-Bu)$_4$NPF$_6$/CH_2Cl_2 vs Ag wire. The saturated Zn^{2+} ion solution was made from $Zn(ClO_4)_2$ dissolving in MeCN solvent, the saturated Cu^{2+} solution was made from $Cu(BF_4)_2$ dissolving in MeCN solvent, and the saturated Cu^{1+} ion solution is made from $Cu(CH_3CN)_4BF_4$ and MeCN.

5-(Tributylstannyl)-2,2-bithiophene. A 1.0 g (6 mmol) sample of 2,2′-bithiophene in 30 mL of THF was treated dropwise with 3.54 mL (6 mmol) of 1.70 M n-butyllithium and stirred for 0.5 h at −78 °C under N_2 atmosphere. A 1.96 mL portion of tributylstannyl chloride (7.2 mmol) was then added to the solution. After the solution was stirred at room temperature for 6 h, the solvent was evaporated and the residue was dissolved in 20 mL of hexane and filtered. The filtrate was evaporated to produce 3.4 g of crude 5-(tributylstannyl)-2,2′-bithiophene as a light yellow liquid for the next reaction. ^{1}H NMR (250 MHz, CDCl$_3$): δ (ppm) 7.27 (d, 1H), 7.15 (2d, 2H), 7.03 (d, 1H), 6.98 (t, 1H), 1.54 (m, 6H), 1.31 (m, 6H), 1.10 (t, 6H), 0.89 (m, 9H). ^{13}C NMR (125 MHz, CDCl$_3$): δ (ppm) 136.28, 127.98, 127.94, 125.19, 124.56, 124.17, 123.97, 123.66, 29.10, 27.50, 13.91, 11.11. MS (FAB): (M^+) found 456, calcd for $C_{20}H_{32}S_2Sn$ 455.28.

5,5′-Bis([2,2′-bithiophen]-5-yl)-2,2′-bipyridine (1). A 0.3 g (1.1 mmol) sample of 5-(tributylstannyl)-2,2′-bithiophene, 0.1 g (0.3 mmol) of 5,5′-dibromo-2,2′-bipyridine, and 0.014 g (5%) of trans-dichlorobis-(triphenylphosphine)palladium (II) catalyst were mixed in 40 mL of DMF and heated at 80−90 °C overnight under argon. After removal of the DMF under vacuum, the resulting solid was chromatographed (silica gel, CH_2Cl_2) to give a yellow compound in 60% yield. For large-scale reactions, recrystallization is suggested. ^{1}H NMR (250 MHz, CDCl$_3$): δ (ppm) 8.92 (d, 2H), 8.42 (d, 2H), 7.98 (dd, 2H), 7.35 (d, 2H), 7.19 (m, 4H), 7.04 (t, 4H). The extremely poor solubility of this compound prevented characterization by ^{13}C NMR. MS (FAB): (M^+) found 485.0268, calcd 485.0274. Anal. Calcd for $C_{26}H_{16}N_2S_4$: C, 64.46; H, 3.33; N, 5.79. Found: C, 63.88; H, 3.43; N 5.49. Mp (under argon): 259 °C, (dec).

2-(Tributylstannyl)-3,4-(ethylenedioxy)thiophene. A 2.0 g (14 mmol) sample of 3,4-(ethylenedioxy)thiophene in 150 mL of dry THF was treated dropwise with 10 mL (16.2 mmol) of 1.6 M n-butyllithium at −78 °C under argon. After the solution was stirred for 0.5 h and warmed to −40 °C, 5.95 g (18.8 mmol) of tributylstannyl chloride was added to the solution, and the new solution was warmed to room temperature. The solvent was removed by rotary evaporation after the solution was stirred for 8 h. The residue was dissolved in hexanes and filtered. The filtrate was dried in vacuum to afford 6.0 g of 2-(tributylstannyl)-3,4-(ethylenedioxy)thiophene as a yellow liquid. The compound was used for the next reaction as obtained, with no further purifications. ^{1}H NMR (250 MHz, CDCl$_3$) δ (ppm) 6.56 (s, 1H); 4.16 (s, 4H); 1.61−1.49 (m, 6H); 1.39−1.22 (m, 6H); 1.09 (t, 9H); 0.90 (q, 6H). ^{13}C NMR (125 MHz, CDCl$_3$): δ (ppm) 147.88, 142.65, 109.08, 105.99, 64.86, 64.80, 29.08, 27.40, 13.79, 10.71. MS: $(M + H)^+$ found 431, calcd for $C_{18}H_{32}O_2SSn$ 430.11

5,5′-Bis(3,4-(ethylenedioxy)thien-2-yl)-2,2′-bipyridine (3). A 0.1 g (0.16 mmol) sample of 5,5′-dibromo-2,2′-bipyridine, 0.4 g (0.5 mmol) of 2-(tributylstannyl)-3,4-(ethylenedioxy)thiophene, and 0.022 g (5%) of trans-dichlorobis(triphenylphosphine)palladium(II) catalyst were mixed in 50 mL of dry DMF and heated to 110°C for 6 h under argon. After removal of the DMF under vacuum, the residue was purified by column chromatography (2% MeOH/CH_2Cl_2) to generate 0.14 g of a yellow solid. Yield: 95%. ^{1}H NMR (250 MHz, DMSO-d_6): δ (ppm) 8.96 (s, 2H); 8.39 (d, 2H, $J = 10$ Hz); 8.14 (d, 2H, $J = 7.5$ Hz); 6.79 (s, 2H); 4.39 (s, 4H), 4.29 (s, 4H). ^{13}C NMR (125 MHz, DMSO-d_6): δ (ppm) 162.26, 155.35, 152.10, 149.79, 143.0, 142.86, 138.93, 130.12, 109.72, 74.82, 73.94. MP (under argon): 228−229 °C. MS (FAB): $(M + H)^+$ found 437.063, calcd for $C_{22}H_{16}N_2O_4S_2$ 436.055.

5,5′-Bis(5-bromo-3,4-(ethylenedioxy)thien-2-yl)-2,2′-bipyridine. A 70 mg (0.16 mmol) sample of 5,5′-bis(3,4-(ethylenedioxy)thienyl)-2,2′-bipyridine was suspended in 10 mL of DMF and stirred for 10 min under reduced-lighting conditions. To the solution was added 57 mg (0.32 mmol) of NBS. Stirring overnight at room temperature resulted in the precipitation of a yellow solid from the solution, which was

collected by filtering and washing with a small amount of acetone. Drying the yellow solid under vacuum provided 70 mg of 5,5′-bis(5-bromo-3,4-(ethylenedioxy)thienyl)-2,2′-bipyridine. Yield: 74%. ^{1}H NMR (250 MHz, DMSO-d_6): δ (ppm) 8.92 (s, 2H); 8.39 (d, 2H, $J =$ 10 Hz); 8.13 (d, 2H, $J = 7.5$ Hz); 4.41 (m, 8H). The poor solubility of this compound precluded obtaining a ^{13}C NMR on this compound. MS (FAB): (M[+]) found 595, calcd for $C_{34}H_{24}N_2O_8S_4$ 594.29. Mp (under argon): 260 °C dec.

5,5′-Bis(3,4:3′,4′-bis(ethylenedioxy)[2,2′-bithiophen]-5-yl)-2,2′-bipyridine (2). A 35 mg (0.06 mmol) sample of 5,5′-bis(5-bromo-3,4-(ethylenedioxy)thienyl)-2,2′-bipyridine, 100 mg (0.24 mmol) of 2-(tri-butylstannyl)-3,4-(ethylenedioxy)thiophene, and 7 mg (10%) of tetra-kis(triphenylphosphine)palladium(0) were refluxed in 30 mL of dry DMF for 6 h under argon. The solvent was removed under vacuum. The resulting red solid was dissolved in CH_2Cl_2 and filtered under argon. The filtrate's volume was reduced to approximately 5 mL, and the brown-yellow product precipitated upon the addition of hexanes to the CH_2Cl_2 solution. The compound was collected and dried to afford 23 mg of 5,5′-bis(3,4:3′,3′-(ethylenedioxy)[2,2′-bithiophen]-5-yl)-2,2′-bipyridine (**2**) as a brown-yellow solid. Yield: 54%. ^{1}H NMR (250 MHz, DMSO-d_6): δ (ppm) 8.98 (s, 2H); 8.39 (d, 2H); 8.13 (d, 2H); 6.66 (s, 2H); 4.45−4.27 (b, 16H). The poor solubility of this compound prevented characterization by ^{13}C NMR. MS (FAB): (M + H^{+}) found 717.0494, calcd for $C_{34}H_{24}N_2O_8S_4$ 716.0417. Mp (under argon): >260 °C.

Rot(1,Zn)(ClO$_4$)$_2$. A 25 mL CH_2Cl_2 solution containing 0.05 g of the macrocyclic phenanthroline[16] and 0.042 g of **1** was added to 0.033 g of Zn(ClO$_4$)$_2$·xH$_2$O in 3 mL of CH$_3$CN, and the mixture was stirred for 2 h at room temperature. After filtering, the solvent was removed, and the residue was dissolved in 20 mL of acetone and filtered. Diethyl ether was added to the red-orange filtrate to precipitate a red-orange solid at 0 °C. Yield: 71%. ^{1}H NMR (500 MHz, acetone-d_6): δ (ppm) 9.23 (d, 2H, $J = 8.5$ Hz); 8.70 (s, 4H); 8.61 (s, 2H); 8.53 (s, 2H); 8.49 (d, 2H, $J = 8.5$ Hz); 7.685 (d, 4H, $J = 2$ Hz); 7.66 (m, 2H); 7.55 (dd, 2H, $J = 4.5$ Hz, $J = 1$); 7.40 (d, 4H, $J = 4$ Hz); 7.15 (m, 2H); 6.63 (d, 4H, $J = 8.5$ Hz); 3.94 (t, 4H, $J = 4.5$ Hz); 3.88 (m, 8H); 3.79 (t, 4H, $J = 4$ Hz); 3.75 (t, 4H, $J = 4$ Hz). ^{13}C NMR (125 MHz, CDCl$_3$): δ (ppm) 160.05, 159.0, 145.5, 145.0, 141.8, 141.25, 141.24, 140.0, 137.5, 136.47, 135.5, 132.01, 129.34, 128.66, 128.11, 127.02, 125.79, 125.58, 124.92, 124.79, 122.57, 115.04, 115.0, 70.87, 70.71, 70.5, 69.34, 68.41. Anal. Calcd for $C_{60}H_{50}N_4O_{14}Cl_2S_4Zn$: C, 54.87; H, 3.84; N, 4.27. Found: C, 54.43; H, 4.17; N, 3.49. Mp (under argon): >260 °C.

Rot(1,Cu)(BF$_4$). This compound was synthesized by the same method as Rot(**1**,Zn)(ClO$_4$)$_2$ in 70% yield as a green-black solid. ^{1}H NMR (250 MHz, acetone-d_6): δ (ppm) 9.37 (d, 2H); 8.89−8.78 (m, 10H); 8.11 (d, 4H); 8.00 (d, 2H); 7.93 (d, 2H); 7.79 (d, 4H); 7.57 (t, 2H), 6.83 (d, 4H); 4.27 (m, 20H). ^{13}C NMR (125 MHz, acetone-d_6): δ (ppm): 160.64, 158.83, 150.44, 145.89, 144.83, 143.18, 138.63, 137.36, 134.56, 132.32, 130.45, 129.28, 127.95, 127.39, 126.68, 126.06, 125.58, 125.56, 123.70, 117.0, 116.90, 114.79, 114.77, 71.75, 71.63, 71.55, 70.28, 69.12. Anal. Calcd for $C_{60}H_{50}N_4O_6S_4BF_4Cu$: C, 59.99; H, 4.20; N, 4.67. Found: 59.92; H, 4.41; N, 4.14. Mp (under argon): 163 °C dec.

Rot(3,Zn)(ClO$_4$)$_2$. This compound was synthesized by the same method as Rot(**1**,Zn)(ClO$_4$)$_2$ in 60% yield as a yellow solid. ^{1}H NMR (500 MHz, acetone-d_6): δ (ppm) 9.25 (d, 2H); 8.63 (s, 2H); 8.55 (m, 8H); 7.67 (d, 2H); 6.78 (s, 2H); 6.61 (d, 4H); 4.35 (m, 8H); 3.85 (m, 20H). [13]C (125 MHz, acetone-d_6): δ (ppm) 161.61, 160.65, 146.89, 146.88, 145.58, 143.72, 143.00, 142.65, 138.16, 133.57, 132.59, 130.56, 129.50, 128.10, 126.38, 123.64, 116.20, 111.81, 103.02, 71.69, 71.52, 70.04, 69.23, 66.24, 65.35, 62.99. Mp (under argon): 175 °C dec.

Rot(2,Zn)(ClO$_4$)$_2$. To a 50 mL air-free Schlenk flask containing 20 mg (0.027 mmol) of **2** and 15.8 mg (0.027 mmol) of the macrocycle phenanthroline[16] was added 25 mL of dry deoxygenated CH$_2$Cl$_2$. The orange-yellow solution was stirred for 10 min under argon, and then 10.4 mg (0.027 mmol) of Zn(ClO$_4$)$_2$ in 2 mL of deoxygenated CH$_3$CN solution was added. The solution turned red immediately, and after the mixture was stirred at room temperature for 10 h, the solvent was removed under vacuum. The crude product was dissolved in 5 mL of acetone under argon and filtered. The red product was precipitated from the filtrate with addition of ether and cooling to 0 °C under argon. A red solid was collected and dried to produce 20 mg of Rot(**2**,Zn). This compound was stored in a refrigerator under argon. ^{1}H NMR (500 MHz, acetone-d_6): δ (ppm) 9.26 (d, 2H, $J = 8.5$ Hz); 8.63 (s, 2H); 8.52 (m, 8H); 7.68 (d, 4H $J = 8.5$ Hz); 6.64 (d, 4H, $J = 8.5$ Hz); 6.58 (s, 2H); 4.44−4.30 (m, 16H); 3.96−3.74 (b, 20H). ^{13}C NMR (125 Mhz, acetone-d_6): δ (ppm) 164.02, 161.68, 156.53, 146.73, 145.00, 142.97, 142.57, 141.50, 141.00, 138.38, 137.29, 132.60, 130.60, 128.13, 126.44, 123.40, 116.68, 116.24, 116.22, 111.00, 109.78, 102.79, 100.609, 71.57, 71.55, 70.02, 70.00, 69.20, 66.39, 66.37, 66.25, 65.54. Mp (under argon): 175 °C dec.

Rot(2,Cu)(BF$_4$). To make Rot(**2**,Cu), we used a method similar to that reported for Rot(**2**,Zn). The compound is brick red in color and was stored in a refrigerator under argon. ^{1}H NMR (300 MHz, acetone-d_6): δ (ppm) 9.25 (d, 2H, $J = 9$ Hz); 8.67 (s, 2H); 8.51(m, 8H), 7.69 (d, 4H, $J = 9$ Hz), 6.65 (d, 4H, $J = 8.1$ Hz); 6.58 (s, 2H); 4.30−4.26 (m, 16H), 3.73 (m, 20H). Mp (under argon): 170 °C dec. The poor solubility of this compound prevented characterization by ^{13}C NMR.

3,4-(Ethylenedioxy)-2,2′-bithiophene. A 2.0 g (14 mmol) sample of EDOT and 1.63 g (28 mmol) of TMEDA were dissolved in 50 mL of dry THF, and the solution was cooled to −10 °C under argon. A 8.8 mL portion of 1.6 M n-BuLi was slowly added to the solution. After being stirred for 30 min, this reaction mixture was transferred to 50 mL of refluxing THF containing 4.97 g (14 mmol) of Fe(acac)$_3$ under argon. The THF was removed after refluxing for 6 h. The resulting red solid was dissolved in CHCl$_3$, and quickly passed through a short bed of silica gel using CHCl$_3$ as eluent. The filtrate was dried and washed with ether. The resulted yellow solid was filtered and dried under vacuum to afford 0.99 g of product. Yield: 99%. ^{1}H NMR (250 MHz, CD$_2$Cl$_2$): δ (ppm) 6.25 (s, 2H), 4.31 (m, 8H), 4.21 (m, 8H). [13]C (125 MHz, acetone-d_6): δ (ppm) 141.23, 137.03, 109.90, 97.53, 64.99, 64.59. GC/MS: found 282, calcd for $C_{12}H_{10}O_4S_2$ 282.00.